ACS Photonics

Article

pubs.acs.org/journal/apchd5

Anomalous Shift Behaviors in the Photoluminescence of Dolmen-Like Plasmonic Nanostructures

Tingting Yin,[†,‡] Zhaogang Dong,[†,§] Liyong Jiang,[†,‡,∥] Lei Zhang,[⊥] Hailong Hu,[○] Cheng-Wei Qiu,[⊥] Joel K. W. Yang,[*,#,§] and Ze Xiang Shen[*,‡,○]

[‡]Centre for Disruptive Photonic Technologies (CDPT), School of Physical and Mathematical Sciences, and [○]Division of Physics and Applied Physics, School of Physical and Mathematical Sciences, Nanyang Technological University, Singapore 637371, Singapore

[§]Institute of Materials Research and Engineering, A*STAR (Agency for Science, Technology and Research), 2 Fusionopolis Way, Innovis, #08-03, Singapore 138634, Singapore

[∥]Department of Physics, School of Science, Nanjing University of Science and Technology, Nanjing 210094, China

[⊥]Department of Electrical and Computer Engineering, National University of Singapore, Singapore 117583, Singapore

[#]Singapore University of Technology and Design, 8 Somapah Road, Singapore 487372, Singapore

Supporting Information

ABSTRACT: Localized surface plasmon resonance (LSPR) on metallic nanostructures is able to enhance photoluminescence (PL) emission significantly. However, the mechanism for anomalous blue-shifted peak of PL emission from metallic nanostructures, relative to the corresponding scattering spectra, is still unclear so far. In this paper, we presented the detailed investigations on both the Lorentz-like PL profile with blue-shifted peak and Fano-like one with almost unshifted dip, as observed on dolmen-like metallic nanostructures. Such anomalous PL emission profile is the product of the density of plasmon states (DoPS) with Lorentz-/Fano-like profile and the population distribution of the relaxed collective free electrons during relaxation. To be more specific, the fast relaxation process of these collective free electrons contributes to the PL shifting characteristics of both Lorentz-like and Fano-like emission profiles. We believed that our results provide a general solid foundation and guidance for analyzing and manipulating the physical processes of the PL emission from various plasmonic nanostructures.

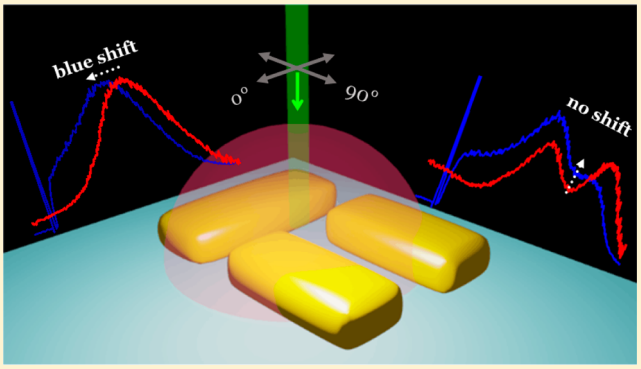

KEYWORDS: *plasmonic nanostructures, photoluminescence, Fano-like resonance, density of plasmon states, blue shift, relaxation*

Photoluminescence (PL) from bulk noble metals and metallic nanostructures has been extensively studied. It reveals that PL from bulk noble metals shares the same mechanism with semiconductors, where a three-step process is involved: (i) Photoexcitation of electron−hole pairs; (ii) Relaxation of excited electrons; and (iii) Recombination of electron−hole pairs.[1,2] Since the recombination rate of the electron−hole pairs is much slower than other nonradiative channels, the quantum efficiency of such luminescence is very low (in order of $\sim 10^{-10}$). On the other hand, PL from metallic nanostrcutures is interpreted due to the radiative decay of localized surface plasmon resonance (LSPR),[3−11] where the corresponding quantum efficiency has been strongly enhanced by million times.[12−14] There is also strong evidence that the time-resolved PL from gold nanoparticles shows ultrafast emission (≤50 fs),[15] comparable with the LSPR dephasing time.[16,17]

PL and absorption are complementary in nature, and it is worth noticing that PL and absorption spectra have distinguished peak positions. In semiconductors and bulk metals, the radiative recombation happens between electrons at the bottom of conduction band and holes on the top of valence band. It implies that PL emissions are always red-shifted as compared to the corresponding absorption edge. Similarly, in metallic nanostructures, the plasmon-contributed PL peak is also red-shifted relative to the absorption edge of *d*−*sp* interband transitions. Recently, a blue-shifted PL peak with respect to the corresponding absorption and scattering of LSPR has been observed in metallic nanostructures.[3,18−21] However, an unambiguous understanding toward such anomalous blue shift characteristic is still missing in the literature so far. Therefore, it is important to address this PL shifting behavior so as to fully understand the PL emission processes on metallic nanostructures.

Received: January 25, 2016
Published: April 25, 2016

DOI: 10.1021/acsphotonics.6b00058
ACS Photonics 2016, 3, 979−984

In this paper, we presented the detailed investigations on the PL and dark-field (DF) scattering[22,23] of dolmen-like nanostructures that consist of a single rod (monomer), supporting a dipolar mode, arranged in perpendicular to two parallel rods (dimer), supporting a quadrupolar mode.[24,25] When the polarization of the excitation laser is parallel to the long axis of dimer, we observed Lorentz-like line shape in both PL and DF scattering spectra, where the PL peak position is blue-shifted relative to the DF scattering peak. When the polarization of the excitation laser is along the long axis of monomer, there is an energy transfer from the radiative dipolar mode on monomer to the nonradiative quadrupolar mode on dimer via near-field coupling. As a result, it gives rise to a sharp quadrupolar resonance in the broad dipolar resonant profile, that is, Fano-like line shape,[26−31] where the resonant dip in both PL and DF scattering spectra emerges at nearly the same wavelength. The transformation of PL from Lorentz-like profile to Fano-like one could be controlled by the polarization configurations and it successfully demonstrates that the intrinsic DoPS will shape the PL profiles.[32−34] Furthermore, we demonstrated that the relaxation process of the excited collective free electrons can be perfectly described by an exponential function, and the fast relaxation process of excited collective free electrons contributes to the anomalous shifting characteristics of both Lorentz-like and Fano-like PL emissions.

RESULTS AND DISCUSSION

Dolmen-like gold nanostructures were fabricated by electron beam lithography (EBL)[35,36] on a bare glass coverslip without any adhesion layer, and the schematic is shown in Figure 1A. The magnified inset shows the corresponding geometrical dimensions of each unit cell. The pitch size is set to be 3 μm along both x- and y-directions, which is much larger than the focused light spot (~1 μm for white light and <0.5 μm for laser). Thus, both the diffraction and intercoupling effects between the unit cells will be ignored. Both PL and DF scattering[37] measurements on the individual dolmen-like nanostructures were carried out on a WITec CRM200 confocal Raman microscopy system.[19] A continuous wave (CW) laser with the wavelength of 532 nm and a broadband light source were used for PL and scattering measurements, respectively. The polarization angles of 0° and 90° are labeled by the green arrows, as shown by the insets in Figure 1B,C.

The blue curve in Figure 1B presents the measured PL spectrum as excited and collected at polarization angle of 0°, which demonstrates a Lorentz-like line shape. The PL peak blue shifts ~20 nm relative to the DF scattering peak (see the red curve in Figure 1B). In comparison, when both excitation and collection polarization angles are set to 90°, a Fano-like PL and DF scattering spectra are obtained with an almost same dip at ~660 nm, as shown by the blue and red curves in Figure 1C. This observation was further confirmed by the additional measurements on three different samples (see more details in Figure S1 of the Supporting Information).

In order to fully understand the blue-shifted peak and almost unshifted dip in Lorentz-like and Fano-like line shape PL spectra, a fundamental physical model is proposed here to visualize the formation process of PL in dolmen-like plasmonic nanostructures, as displayed in Figure 2A.

i. Excitation. Both the bound electrons and the collective free electrons under Fermi level are excited to a state with the same energy level as the excitation laser of 532 nm (~2.33 eV).[3,12,38,39] The contribution of the excited bound electrons in the d-valence band to this PL spectra is 30 times weaker than collective free electrons for the 532 nm laser excitation (refer to Figure S3 for details).

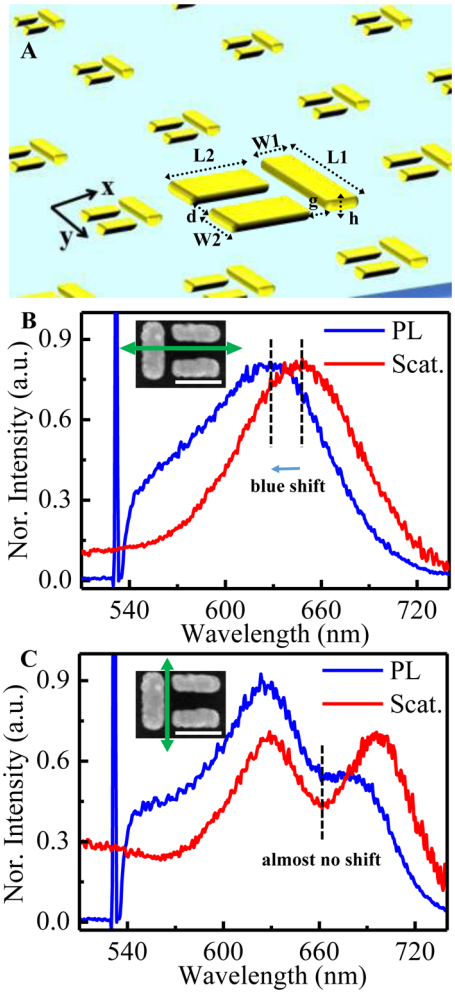

Figure 1. (A) Schematic of the dolmen-like nanostructures fabricated on glass substrate with the geometrical parameters: L1 = 120 nm, W1 = 50 nm, L2 = 100 nm, W2 = 40 nm, d = 40 nm, g = 15 nm, and h = 40 nm. The pitch size is 3 μm along both x- and y-directions. (B, C) Measured PL and DF scattering spectra of the individual dolmen-like nanostructures with excitation-collection polarization of 0−0° and 90−90°, respectively, as specified by green arrows in the magnified SEM images with a scale bar of 100 nm.

ii. Relaxation. The excited collective free electrons will relax from the initial excited state into the continuous plasmon states (including the plasmon resonance state), where the population of excited collective free electrons will be redistributed with a relaxation process as illustrated by the blue solid line in Figure 2A,B.

iii. Plasmon-Modulated Emission for Lorentz-Like Line Shape PL. For the excitation-collection configuration of 0−0°, the excited collective free electrons will relax into the broad bright plasmon states with Lorentz-like distributed DoPS (see details in Figure S2a), as represented by the dark green dashed line in Figure 2A,B. The radiative decay of plasmon resonance leads to the PL profile following closely to that of the DF scattering. Hence, the observed PL intensity is proportional to the product of population redistribution and DoPS, that is, I_{PL} ~ DoPS and population. The population redistribution skewed strongly toward to the high energy side is responsible

DOI: 10.1021/acsphotonics.6b00058
ACS Photonics 2016, 3, 979−984

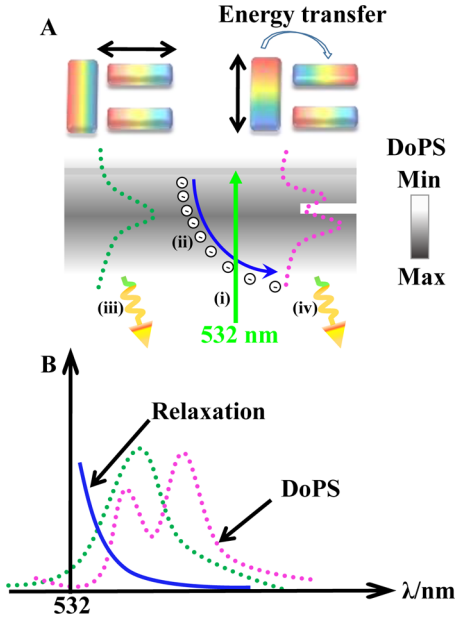

Figure 2. Proposed mechanism for PL emission process on the dolmen-like plasmonic nanostructures. (A) Schematic illustration on the physical process of PL on the dolmen-like nanostructures: (i) Excitation of electrons; (ii) Relaxation of excited collective free electrons; (iii, iv) Plasmon-modulated light re-emission. The dark green and pink dashed lines represent the profiles of DoPS and the grayscale map represents the intensity distribution of DoPS in frequency space. (B) Qualitative description of the PL spectrum: the product of DoPS and population redistribution of relaxed collective free electrons. DoPS with Lorentz-like profile (the dark green dashed line) and Fano-like profile (the pink dashed line) represents the probability for PL emission, which can be characterized by the scattering spectrum. Population redistribution (the blue solid line) represents the number of relaxed collective electrons as occupied in different plasmon states, which has an exponential decay as a function of frequency (wavelength).

for the blue shift of PL peak relative to the corresponding scattered peak, as shown in Figure 2B.

iv. Plasmon-Modulated Emission for Fano-Like Line Shape PL. For the excitation-collection configuration of 90−90°, the radiative emission through the broad bright plasmon mode sustained in the monomer will be modulated by Fano-like DoPS. As a perturbation, the narrow dark mode sustained in the dimer will destructively interact with the bright mode in monomer to generate a Fano-like DoPS (see details in Figure S2c), as represented by the pink dashed line in Figure 2A,B. As a result, the light emission from the monomer will be reshaped, and the dip position in both PL and scattering spectra occurs in almost the same position, which is corresponding to the dark plasmon mode energy.

To demonstrate the proposed physical mechanism is valid independent of specific plasmon resonant peak and dip position, we plot the peak and dip shift as a function of plasmon resonant position (refer to Figure S1d for details).

Based on the physical mechanism proposed above, a model $I_{PL}(\omega) = I_{scat}(\omega)N_{electron}(\omega)$ was introduced here to quantitatively describe the Lorentz-like and Fano-like line shape PL generation process. $I_{scat}(\omega)$ is the scattering spectrum, which can be used to characterize DoPS. $N_{electron}(\omega)$ is the strength of relaxed collective free electrons as occupied in plasmon states.

The measured Lorentz-like PL spectrum can be further evaluated as the form:

$$I_{PL}(\omega) = \left[I_0 + A_0 \left(\frac{1}{\pi} \times \frac{\frac{1}{2}\Gamma}{(\omega - \omega_c)^2 + \left(\frac{1}{2}\Gamma\right)^2} \right) \right] \times N_0 \exp^{-(\omega-\omega_0)/\xi} \quad (1)$$

where the Lorentz function, $I_{scat}(\omega) = I_0 + A_0 \left(\frac{1}{\pi} \times \frac{\frac{1}{2}\Gamma}{(\omega - \omega_c)^2 + \left(\frac{1}{2}\Gamma\right)^2} \right)$, indicates the DoPS of the bright plasmon dipolar mode in the dimer. ω_c is the plasmon resonant frequency. Γ specifies the line width of scattering spectrum. I_0 and A_0 represent the background and amplitude. Then, the DoPS distribution could be obtained via fitting the measured scattering spectrum, as shown by the red solid line in Figure 3A, and the corresponding fitted parameters are listed in the first row of Table 1.

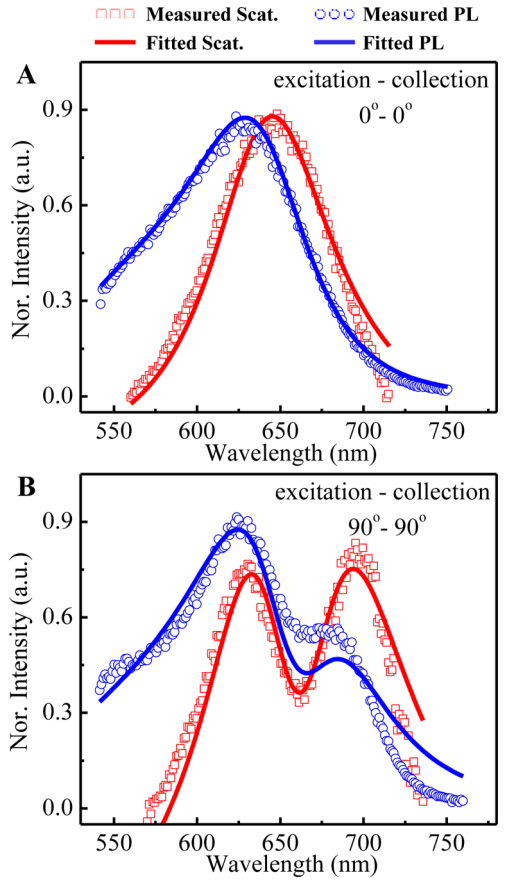

Figure 3. (A, B) Measured scattering (scat) spectra (red boxes) and PL spectra (blue circles) under excitation-collection configuration of 0−0° and 90−90°, respectively. The corresponding fitted curves to the data are indicated by the solid lines.

In particular, the relaxation of the excited collective free electrons is assumed to be simply exponential and this decay

Table 1. Fitted Parameters of Lorentz-Like Line-Shape Scattering (scat) and PL Spectrum

	I_0	A_0[a]	ω_c (THz)	Γ (THz)	ξ (THz)
scat	0.03	17.6	464.9	66.0	
PL	0.19	219.7	464.9	66.0	47.4

[a]The fitting parameter of $A_0 = A_0 \times N_0$ for PL curve fitting.

DOI: 10.1021/acsphotonics.6b00058
ACS Photonics 2016, 3, 979−984

starts immediately after the excitation. The relaxation response function is described by the second term, $N_{electron}(\omega) = N_0 \exp^{-(\omega-\omega_0)/\xi}$, where N_0 is the initial strength of the excited collective free electrons. ξ is denoted as relaxation parameter and the initial frequency ω_0 is 564 THz (i.e., 532 nm). This relaxation response function is also demonstrated to be applicable in classical individual gold nanorod, as shown in Figure S4. During the fitting process, we first fixed ω_c, Γ, and ω_0 values and fitted the PL curve to obtain other parameters. The fitted result is shown by the blue solid line in Figure 3A and the fitted parameters are listed in the second row of Table 1, respectively. Equation 1 clearly illustrates the effect of the excited collective free electron relaxation on the blue-shifted optical behaviors (~20 nm) in Lorentz-like line shape PL spectrum. In addition, the same line width in both PL and scattering spectra demonstrates that the PL emission process on dolmen-like gold nanostructures is through plasmon radiative decay channel, instead of the direct recombination of electron−hole pairs as in traditional semiconductors and bulk metals. Nevertheless, the relaxation process on plasmonic nanostructures is similar to that in bulk metals, as evidenced by the perfect agreement between the measured data and the fitted results with an exponential decay as shown in Figure 4.

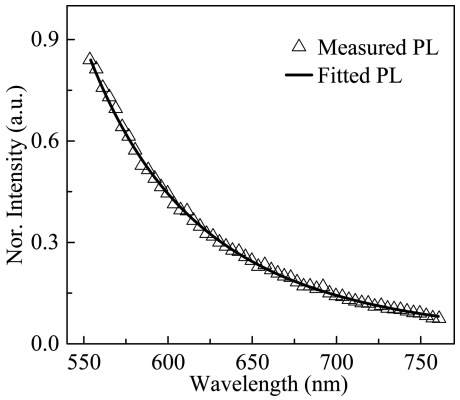

Figure 4. Measured PL spectrum of the flat gold film (black triangle). The corresponding fitted curve to the data is represented by the solid black line.

Here, the classical two-oscillator model is used to quantitatively describe the plasmonic Fano-like resonance properties in our dolmen-like nanostructures.[40,41] The bright mode in monomer is regarded as oscillator 1, which will be driven by incident electromagnetic field $E(t)$. The dark mode in dimer is represented by oscillator 2, which can only be driven by oscillator 1 via near-field coupling. Thus, the charge oscillations $x_1(t)$ and $x_2(t)$ satisfy the differential function:

$$\ddot{x}_1(t) + \gamma_1\dot{x}_1(t) + \omega_c^2 x_1(t) - \kappa\dot{x}_2(t) = E(t) \quad (2)$$

$$\ddot{x}_2(t) + \gamma_2\dot{x}_2(t) + (\omega_c + \delta)^2 x_2(t) - \kappa\dot{x}_1(t) = 0 \quad (3)$$

where x_1, x_2, and ω_c ($\omega_c + \delta$) are the amplitudes and the resonant frequency of the bright and dark mode in oscillators 1 and 2, respectively. γ_1, γ_2, and κ are the damping rate and the coupling strength of the two resonators.[26,30,42] After some manipulation and approximation, we can obtain the amplitude of oscillator 1. Then, the scattering intensity as a function of frequency is obtained via modulus square of x_1:

$$I_{scat}(\omega) = I_0 + A_0\Big[[(\omega - \omega_c - \delta)^2 + \gamma_2^2/4] / [((\omega - \omega_c) \times (\omega - \omega_c - \delta) - \frac{\gamma_1 \times \gamma_2}{4} - \frac{\kappa^2}{4})^2 + (\frac{\gamma_1}{2} \times (\omega - \omega_c - \delta) + \frac{\gamma_2}{2} \times (\omega - \omega_c))^2]\Big] \quad (4)$$

The fitted DoPS is described by the red solid line as shown in Figure 3B and the corresponding fitted parameters are listed in the first row of Table 2. Using the same treatment as in Lorentz-like line shape PL data analysis, that is, $I_{PL}(\omega) = I_{scat}(\omega)N_{electron}(\omega)$, we successfully fit the Fano-like line shape PL spectrum with almost the same dip as measured in the scattering spectrum, as shown by the blue solid line in Figure 3B. Specifically, through comparing the corresponding fitted values of γ_1 and γ_2, as listed in Table 2, it is obvious that the dark mode is much narrower than the bright mode and the relaxation response function keeps relatively flat in such narrow frequency span. As a result, it leads to an almost unshifted dip in the PL spectrum.

Last, we did the PL measurement on the bulk gold film as excited by 532 nm laser. To be more specific, we introduce the exponential function, $N_0 \exp^{-(\omega-\omega_0)/\xi}$, that is, the second term as shown in eq 1, to fit the relaxation process of the excited electrons in bulk metals, where ω_0 is still the excitation laser frequency. It confirms that the pure electron behavior after excitation in bulk metals is exponential as a function of energy, as demonstrated in Figure 4.

CONCLUSIONS

To conclude, this paper presents that controlling the excitation-collection polarization configuration is able to achieve both the Lorentz-like line shape PL with blue-shifted peak and Fano-like line shape PL with almost unshifted dip, from the dolmen-like plasmonic nanostructures. A physical model has been presented to describe that the PL from metallic nanostructures is the product of DoPS and population redistribution during the relaxation process of the excited collective free electrons. It was demonstrated that DoPS, as represented by scattering spectrum, can reshape the PL emission profile, and the population distribution of the relaxed collective free electrons contributes to the blue-shifted peak in Lorentz-like PL emission and stable dip in Fano-like PL emission. Our results provide a solid foundation for the further analysis toward plasmon-dominated light re-emission process in more complex and hybridized metallic nanostructures.

Table 2. Fitted Parameters of Fano-Like Line-Shape Scattering (scat) and PL Spectrum

	I_0	A_0[a]	dip (THz)	γ_1 (THz)	γ_2 (THz)	δ (THz)	κ (THz)	ξ (THz)
scat	0.02	115	453.7	75	30	0.5	31	
PL	0.09	2466.8	453.7	75	30	0.5	31	64.3

[a]The fitting parameter of $A_0 = A_0 \times N_0$ for PL curve fitting.

DOI: 10.1021/acsphotonics.6b00058
ACS Photonics 2016, 3, 979−984

METHODS

Fabrication. Gold dolmen-like plasmonic nanostructures were fabricated on glass substrate with a thickness of 0.17 mm using electron-beam lithography (EBL) and lift-off process. First, 50 nm thick PMMA resist was spin-coated onto the substrate at 4k rpm, and the PMMA resist has a molecular weight of 950k, with a centration of ∼1.67% as dissolved in anisole solvent. Then, the glass substrate was baked on a hot plate at 180 °C for 120 s in order to evaporate the residual solvent. EBL was done in the Elionix ELS-7000 system with an electron-beam current of 100 pA and an accelerating voltage of 100 kV. An optimized dose was used to expose the PMMA resist. After exposure, the samples were developed with the MIBK/IPA (1:3) developer at low temperature of −10 °C for 15 s and followed by the nitrogen blown dry.[36] A 40 nm thick gold layer was deposited by the electron-beam evaporator. The working pressure of $\sim 5 \times 10^{-7}$ Torr was maintained during the whole evaporation process, and the temperature of the sample chamber was kept at 25 °C. To obtain more uniform gold film, the sample holder was rotated at 50 rpm during evaporation process. Lift-off process was carried out by immersing samples in *N*-methylpyrrolidone (NMP) solvent at elevated temperature of 60 °C.

Optical Measurements. Both the DF scattering and PL measurements were implemented by the WITec CRM200 confocal Raman microscopy system. For the DF scattering measurements, a halogen lamp (15 V, 150 W, 3100 K) as the white light source can illuminate the sample uniformly via a dark-field objective lens (Zeiss Epiplan, 100×, N.A. = 0.75), which is also used to collect the elastic scattering light. During the PL measurements, a linearly polarized CW laser with a wavelength of 532 nm was focused on the surface of the individual nanoparticles through the same objective lens as scattering measurements. The laser power on the sample is 50 μW. Both the DF scattering and PL spectra were dispersed by a 150 lines/mm grating and detected using a TE-cooled CCD (Andor DV 401-BV-351). To get a good signal-to-noise ratio, we set the integration time in scattering measurements as 20 s and in PL measurements as 10 s, respectively.

Simulation. All the simulations were performed using the commercial finite-difference time-domain (FDTD) software Lumerical. In simulations, an isolated dolmen nanostructure on quartz substrate was enclosed by perfectly matched layers (PML) along all the directions. Total-field scattered-field (TFSF) was used as the incidence. The polarization and incident direction was indicated in Figure S2c for the excitation of bright mode (red) and dark mode (black). The dielectric functions of gold and SiO_2 were described by fitting the gold-Palik and SiO_2-Palik database in Lumerical's material library. The corner of each nanorod was rounded with a radius 15 nm to mimic the real cases. All the charge distributions were plotted at the surface of structures.

ASSOCIATED CONTENT

Supporting Information

The Supporting Information is available free of charge on the ACS Publications website at DOI: 10.1021/acsphotonics.6b00058.

(S1) The additional measured PL and DF scattering data obtained from three different sample arrays. (S2) Calculated profile and morphology of Lorentz-like and Fano-like DoPS, respectively. (S3) Comparison the PL intensity from Au film and Au dolmen nanostructures under 532 nm laser excitation. (S4) The fitted curves to the measured PL and DF scattering data of single Au nanorod by using the proposed mathematical model (PDF).

AUTHOR INFORMATION

Corresponding Authors

*E-mail: joel_yang@sutd.edu.sg.
*E-mail: zexiang@ntu.edu.sg.

Author Contributions

†These authors contributed equally to this work.

Notes

The authors declare no competing financial interest.

ACKNOWLEDGMENTS

This work was sponsored by Singapore Ministry of Education Academic Research Fund Tier 3 (Grant Number MOE2011-T3-1-005). In addition, Z.D. and J.K.W.Y. would like to acknowledge the funding support from the Agency for Science, Technology and Research (A*STAR) Young Investigatorship (Grant Number 0926030138), SERC (Grant Number 092154099), National Research Foundation (Grant Number NRF-CRP 8-2011-07), and A*STAR-JCO under project number 1437C00135.

REFERENCES

(1) Mooradian, A. Photoluminescence of Metals. *Phys. Rev. Lett.* **1969**, *22*, 185−187.

(2) Boyd, G. T.; Yu, Z. H.; Shen, Y. R. Photoinduced Luminescence from the Noble Metals and Its Enhancement on Roughened Surfaces. *Phys. Rev. B: Condens. Matter Mater. Phys.* **1986**, *33*, 7923−7936.

(3) Beversluis, M. R.; Bouhelier, A.; Novotny, L. Continuum Generation from Single Gold Nanostructures through near-Field Mediated Intraband Transitions. *Phys. Rev. B: Condens. Matter Mater. Phys.* **2003**, *68*, 115433.

(4) Dulkeith, E.; Niedereichholz, T.; Klar, T. A.; Feldmann, J.; von Plessen, G.; Gittins, D. I.; Mayya, K. S.; Caruso, F. Plasmon Emission in Photoexcited Gold Nanoparticles. *Phys. Rev. B: Condens. Matter Mater. Phys.* **2004**, *70*, 205424.

(5) Bouhelier, A.; Bachelot, R.; Lerondel, G.; Kostcheev, S.; Royer, P.; Wiederrecht, G. P. Surface Plasmon Characteristics of Tunable Photoluminescence in Single Gold Nanorods. *Phys. Rev. Lett.* **2005**, *95*, 267405.

(6) Tcherniak, A.; Dominguez-Medina, S.; Chang, W. S.; Swanglap, P.; Slaughter, L. S.; Landes, C. F.; Link, S. One-Photon Plasmon Luminescence and Its Application to Correlation Spectroscopy as a Probe for Rotational and Translational Dynamics of Gold Nanorods. *J. Phys. Chem. C* **2011**, *115*, 15938−15949.

(7) Shahbazyan, T. V. Theory of Plasmon-Enhanced Metal Photoluminescence. *Nano Lett.* **2013**, *13*, 194−198.

(8) Andersen, S. K. H.; Pors, A.; Bozhevolnyi, S. I. Gold Photoluminescence Wavelength and Polarization Engineering. *ACS Photonics* **2015**, *2*, 432−438.

(9) Verellen, N.; Denkova, D.; Clercq, B. D.; Silhanek, A. V.; Ameloot, M.; Dorpe, P. V.; Moshchalkov, V. V. Two-Photon Luminescence of Gold Nanorods Mediated by Higher Order Plasmon Modes. *ACS Photonics* **2015**, *2*, 410−416.

(10) Wan, A.; Wang, T.; Yin, T. T.; Li, A. R.; Hu, H. L.; Li, S. Z.; Shen, Z. X.; Nijhuis, C. A. Plasmon-Modulated Photoluminescence of Single Gold Nanobeams. *ACS Photonics* **2015**, *2*, 1348−1354.

(11) Dong, Z. G.; Asbahi, M.; Lin, J.; Zhu, D.; Wang, Y. M.; Hippalgaonkar, K.; Chu, H.-S.; Goh, W. P.; Wang, F. K.; Huang, Z. W.; Yang, J. K. W. Second-Harmonic Generation from Sub-5 Nm

DOI: 10.1021/acsphotonics.6b00058
ACS Photonics 2016, 3, 979−984

Gaps by Directed Self-Assembly of Nanoparticles onto Template-Stripped Gold Substrates. *Nano Lett.* **2015**, *15*, 5976−5981.
(12) Lumdee, C.; Yun, B. F.; Kik, P. G. Gap-Plasmon Enhanced Gold Nanoparticle Photoluminescence. *ACS Photonics* **2014**, *1*, 1224−1230.
(13) Mohamed, M. B.; Volkov, V.; Link, S.; El-Sayed, M. A. The 'Lightning' Gold Nanorods: Fluorescence Enhancement of over a Million Compared to the Gold Metal. *Chem. Phys. Lett.* **2000**, *317*, 517−523.
(14) Wu, X.; Ming, T.; Wang, X.; Wang, P. N.; Wang, J. F.; Chen, J. Y. High-Photoluminescence-Yield Gold Nanocubes: For Cell Imaging and Photothermal Therapy. *ACS Nano* **2010**, *4*, 113−120.
(15) Varnavski, O. P.; Goodson, T.; Mohamed, M. B.; El-Sayed, M. A. Femtosecond Excitation Dynamics in Gold Nanospheres and Nanorods. *Phys. Rev. B: Condens. Matter Mater. Phys.* **2005**, *72*, 235405.
(16) Klar, T.; Perner, M.; Grosse, S.; von Plessen, G.; Spirkl, W.; Feldmann, J. Surface-Plasmon Resonances in Single Metallic Nanoparticles. *Phys. Rev. Lett.* **1998**, *80*, 4249−4252.
(17) Sonnichsen, C.; Franzl, T.; Wilk, T.; von Plessen, G.; Feldmann, J.; Wilson, O.; Mulvaney, P. Drastic Reduction of Plasmon Damping in Gold Nanorods. *Phys. Rev. Lett.* **2002**, *88*, 077402.
(18) Yorulmaz, M.; Khatua, S.; Zijlstra, P.; Gaiduk, A.; Orrit, M. Luminescence Quantum Yield of Single Gold Nanorods. *Nano Lett.* **2012**, *12*, 4385−4391.
(19) Hu, H. L.; Duan, H. G.; Yang, J. K.; Shen, Z. X. Plasmon-Modulated Photoluminescence of Individual Gold Nanostructures. *ACS Nano* **2012**, *6*, 10147−10155.
(20) Fang, Y.; Chang, W. S.; Willingham, B.; Swanglap, P.; Dominguez-Medina, S.; Link, S. Plasmon Emission Quantum Yield of Single Gold Nanorods as a Function of Aspect Ratio. *ACS Nano* **2012**, *6*, 7177−7184.
(21) Huang, D.; Byers, C. P.; Wang, L. Y.; Hoggard, A.; Hoener, B.; Dominguez-Medina, S.; Chen, S. S.; Chang, W. S.; Landes, C. F.; Link, S. Photoluminescence of a Plasmonic Molecule. *ACS Nano* **2015**, *9*, 7072−7079.
(22) Sherry, L. J.; Chang, S.-H.; Schatz, G. C.; Van Duyne, R. P.; Wiley, B. J.; Xia, Y. Localized Surface Plasmon Resonance Spectroscopy of Single Silver Nanocubes. *Nano Lett.* **2005**, *5*, 2034−2038.
(23) Jiang, L. Y.; Yin, T. T.; Dong, Z. G.; Liao, M. Y.; Tan, S. J.; Goh, X. M.; Allioux, D.; Hu, H. L.; Li, X. Y.; Yang, J. K. W.; Shen, Z. X. Accurate Modeling of Dark-Field Scattering Spectra of Plasmonic Nanostructures. *ACS Nano* **2015**, *9*, 10039−10046.
(24) Zhang, S.; Genov, D. A.; Wang, Y.; Liu, M.; Zhang, X. Plasmon-Induced Transparency in Metamaterials. *Phys. Rev. Lett.* **2008**, *101*, 047401.
(25) Verellen, N.; Sonnefraud, Y.; Sobhani, H.; Hao, F.; Moshchalkov, V. V.; Van Dorpe, P.; Nordlander, P.; Maier, S. A. Fano Resonances in Individual Coherent Plasmonic Nanocavities. *Nano Lett.* **2009**, *9*, 1663−1667.
(26) Liu, N.; Langguth, L.; Weiss, T.; Kastel, J.; Fleischhauer, M.; Pfau, T.; Giessen, H. Plasmonic Analogue of Electromagnetically Induced Transparency at the Drude Damping Limit. *Nat. Mater.* **2009**, *8*, 758−762.
(27) Luk'yanchuk, B.; Zheludev, N. I.; Maier, S. A.; Halas, N. J.; Nordlander, P.; Giessen, H.; Chong, C. T. The Fano Resonance in Plasmonic Nanostructures and Metamaterials. *Nat. Mater.* **2010**, *9*, 707−715.
(28) Liu, N.; Hentschel, M.; Weiss, T.; Alivisatos, A. P.; Giessen, H. Three-Dimensional Plasmon Rulers. *Science* **2011**, *332*, 1407−1410.
(29) Chang, W.-S.; Lassiter, J. B.; Swanglap, P.; Sobhani, H.; Khatua, S.; Nordlander, P.; Halas, N. J.; Link, S. A Plasmonic Fano Switch. *Nano Lett.* **2012**, *12*, 4977−4982.
(30) Gallinet, B.; Siegfried, T.; Sigg, H.; Nordlander, P.; Martin, O. J. F. Plasmonic Radiance: Probing Structure at the Ångström Scale with Visible Light. *Nano Lett.* **2013**, *13*, 497−503.
(31) Fan, J. A.; Bao, K.; Wu, C.; Bao, J. M.; Bardhan, R.; Halas, N. J.; Manoharan, V. N.; Shvets, G.; Nordlander, P.; Capasso, F. Fano-Like Interference in Self-Assembled Plasmonic Quadrumer Clusters. *Nano Lett.* **2010**, *10*, 4680−4685.
(32) Frimmer, M.; Coenen, T.; Koenderink, A. F. Signature of a Fano Resonance in a Plasmonic Metamolecule's Local Density of Optical States. *Phys. Rev. Lett.* **2012**, *108*, 077404.
(33) Viarbitskaya, S.; Teulle, A.; Marty, R.; Sharma, J.; Girard, C.; Arbouet, A.; Dujardin, E. Tailoring and Imaging the Plasmonic Local Density of States in Crystalline Nanoprisms. *Nat. Mater.* **2013**, *12*, 426−432.
(34) Chen, W.-L.; Lin, F.-C.; Lee, Y.-Y.; Li, F.-C.; Chang, Y.-M.; Huang, J.-S. The Modulation Effect of Transverse, Antibonding, and Higher-Order Longitudinal Modes on the Two-Photon Photoluminescence of Gold Plasmonic Nanoantennas. *ACS Nano* **2014**, *8*, 9053−9062.
(35) Duan, H. G.; Hu, H. L.; Kumar, K.; Shen, Z. X.; Yang, J. K. Direct and Reliable Patterning of Plasmonic Nanostructures with Sub-10-Nm Gaps. *ACS Nano* **2011**, *5*, 7593−7600.
(36) Dong, Z. G.; Bosman, M.; Zhu, D.; Goh, X. M.; Yang, J. K. Fabrication of Suspended Metal−Dielectric−Metal Plasmonic Nanostructures. *Nanotechnology* **2014**, *25*, 135303.
(37) Hu, M.; Novo, C.; Funston, A.; Wang, H. N.; Staleva, H.; Zou, S. L.; Mulvaney, P.; Xia, Y. N.; Hartland, G. V. Dark-Field Microscopy Studies of Single Metal Nanoparticles: Understanding the Factors That Influence the Linewidth of the Localized Surface Plasmon Resonance. *J. Mater. Chem.* **2008**, *18*, 1949−1960.
(38) Zhang, T.; Lu, G.; Shen, H.; Shi, K.; Jiang, Y.; Xu, D.; Gong, Q. Photoluminescence of a Single Complex Plasmonic Nanoparticle. *Sci. Rep.* **2014**, *4*, 3867.
(39) Jiang, L. Y.; Yin, T. T.; Dong, Z. G.; Hu, H. G.; Liao, M. Y.; Allioux, D.; Tan, S. J.; Goh, X. M.; Li, X. Y.; Yang, J. K. W.; Shen, Z. X. Probing Vertical and Horizontal Plasmonic Resonant States in the Photoluminescence of Gold Nanodisks. *ACS Photonics* **2015**, *2*, 1217−1223.
(40) Joe, Y. S.; Satanin, A. M.; Kim, C. S. Classical Analogy of Fano Resonances. *Phys. Scr.* **2006**, *74*, 259−266.
(41) Lovera, A.; Gallinet, B.; Nordlander, P.; Martin, O. J. F. Mechanisms of Fano Resonances in Coupled Plasmonic Systems. *ACS Nano* **2013**, *7*, 4527−4536.
(42) Gu, J. Q.; Singh, R.; Liu, X. J.; Zhang, X. Q.; Ma, Y. F.; Zhang, S.; Maier, S. A.; Tian, Z.; Azad, A. K.; Chen, H. T.; Taylor, A. J.; Han, J. G.; Zhang, W. L. Active Control of Electromagnetically Induced Transparency Analogue in Terahertz Metamaterials. *Nat. Commun.* **2012**, *3*, 1151.

DOI: 10.1021/acsphotonics.6b00058
ACS Photonics 2016, 3, 979−984